Injection of midinfrared surface plasmon polaritons with an integrated device

J.-P. Tetienne,[1] A. Bousseksou,[1,a)] D. Costantini,[1] R. Colombelli,[1,b)] A. Babuty,[2] I. Moldovan-Doyen,[2] Y. De Wilde,[2] C. Sirtori,[3] G. Beaudoin,[4] L. Largeau,[4] O. Mauguin,[4] and I. Sagnes[4]

[1]*Institut d'Electronique Fondamentale, Univ. Paris Sud, UMR8622 CNRS, 91405 Orsay, France*
[2]*Institut Langevin, ESPCI ParisTech, CNRS UMR 7587, 75231 Paris, France*
[3]*Laboratoire MPQ, University Paris Diderot, CNRS UMR7612, 75013 Paris, France*
[4]*Laboratoire de Photonique et de Nanostructures, CNRS UPR20, 91460 Marcoussis, France*

(Received 28 July 2010; accepted 29 October 2010; published online 24 November 2010)

We demonstrate a compact, integrated device in which surface plasmon polaritons (SPPs) are injected into a passive metal waveguide. We directly excite a SPP mode at a metal-air interface using a room-temperature midinfrared quantum cascade laser which is integrated onto the microchip. The SPP generation relies on end-fire coupling and is demonstrated via both far-field and near-field imaging techniques in the midinfrared. On one hand, a metallic diffraction grating is used to scatter in the far-field a portion of the propagating SPPs, thus allowing their detection with a microbolometer camera. On the other hand, direct images of the generated SPPs in the near-field were collected with a scanning optical microscope. © *2010 American Institute of Physics*. [doi:10.1063/1.3519985]

Surface plasmon polaritons (SPPs) are electromagnetic (EM) modes which are bound to a metal-dielectric interface, along which they propagate while being evanescently confined in the direction normal to the interface. Unlike diffraction-limited photons, SPPs have dispersion properties at visible and near-infrared frequencies which lead to subwavelength confinement of the fields. This makes them appealing for prospective data storage applications[1,2] and micro-/nano-optics for telecommunications.[3] Due to the dispersion of the refractive index of real metals, these properties do not hold in the midinfrared (mid-IR) range of the EM spectrum, but can be retrieved by properly structuring the metal surface.[4] This could open interesting possibilities for potential promising applications as tools for near-field microscopy.[5]

The excitation of SPPs with a compact device is a real challenge[6] due to the need of providing the missing momentum between free photons and SPPs of the same frequency. Recently, we have demonstrated an electrically pumped compact device for the generation of mid-IR SPPs based on a semiconductor quantum cascade (QC) laser with an asymmetric optical waveguide and a top metal grating.[7]

In this letter, we present a different approach for SPP generation, relying on end-fire coupling of a standard, mid-IR QC laser which is directly integrated onto the semiconductor chip. A metal strip is evaporated in the near-field of the QC laser facet, allowing direct excitation of a SPP mode onto the metal-air interface. Note that a similar approach has been recently employed in Ref. 8 at an operating wavelength of 1.46 μm. The interest of our work is also linked to the unavailability of cheap optical fibers operating at mid-IR frequencies, while at telecom wavelengths, ($1.3\ \mu m < \lambda < 1.55\ \mu m$) excitation of SPPs can be achieved for instance by fiber end-coupling.[9] An integrated device for mid-IR SPP generation which can be easily integrated onto a chip is therefore a useful tool for fundamental studies of mid-IR plasmonics.

Figure 1(a) shows a schematic cross section of our device, which explains its operating principle. A standard mid-IR QC laser, designed for nominal emission at $\lambda_0 \approx 7.5\ \mu m$, is used to generate transverse magnetic (TM) polarized light. A gold metal strip is located in proximity to the output facet of the semiconductor laser, at a distance smaller than the wavelength ($<2\ \mu m$). Note that this is different

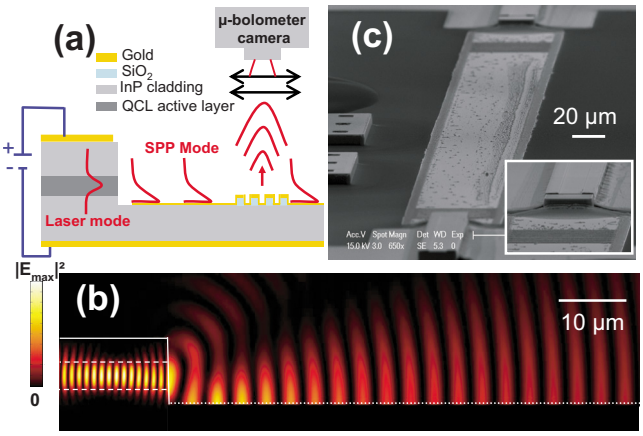

FIG. 1. (Color online) (a) Schematic cross section of the device. A gold strip is evaporated at a subwavelength distance from the dry-etched QC laser facet. A metal grating on the SPP-carrying strip scatters a portion of the SPPs, thereby permitting their observation in the far-field using a μ-bolometer camera. (b) Two-dimensional numerical simulation of the electric field intensity. The dotted white line shows the gold-air interface, the solid white line shows the end-laser facet geometry, and the dashed white line corresponds to the QCL active layer and the InP cladding layers interfaces. The diffraction metallic gratings are not included in the presented numerical simulation. The TM_0 mode of the QC laser, at $\lambda_0 = 7.5\ \mu m$, is used as the excitation. A SPP propagating at the gold-air interface is excited via end-fire coupling. (c) Scanning electron microscopy image of a typical device. Inset: close-up of the region near the laser facet.

a)Electronic mail: adel.bousseksou@u-psud.fr.
b)Electronic mail: raffaele.colombelli@u-psud.fr.

from what is presented in Ref. 8, where a gold plasmonic waveguide is located at a few wavelengths distance from the facet of a semiconductor laser. The laser output is directly coupled into the SPP mode bound at the gold-air interface. Diffraction, second-order gratings fabricated on the gold strip, allow one to partially diffract the propagating SPPs in the far-field. Each grating acts as a *localized probe* of the SPP presence: it permits its unambiguous detection using a microbolometer camera. Figure 1(b) shows an electromagnetic numerical simulation of the system, performed with a finite-element approach using a commercial software.[10] The fundamental TM_0 waveguide mode of the laser, at $\lambda_0 = 7.5\ \mu m$, is employed as the excitation. The simulation shows that an electromagnetic mode, whose electric field is clearly bound at the metal-air interface, propagates on the passive metal waveguide.

Figure 1(c) shows a scanning electron microscopy image of a typical processed device where two diffraction gratings are implemented at the beginning and the end of the metallic strip. The QC laser heterostructure has been grown in a vertical low pressure VEECO-D-180 turbo disk reactor (70 Torr), by using trimethylindium, trimethylaluminium, trimethylgallium, arsine, and phosphine as precursors and hydrogen (H_2) as carrier gas.[11] It contains 50 repetitions of a two-phonon-resonance active region designed for nominal emission at $\lambda_0 = 7.5\ \mu m$. The 2.6-μm-thick active region, whose details are reported in Ref. 12, is sandwiched between two 0.5-μm-thick low-doped InGaAs cladding layers, thereby forming a 3.6-μm-thick waveguide core. The InP upper cladding is 3.5-μm-thick, while the sample is grown on a low-doped ($n = 10^{17}\ cm^{-3}$) InP substrate. Standard laser ridges (22-μm-wide, 1.5-mm-long, and 7-μm-high) were defined using inductively coupled plasma (ICP) etching,[13] employing a 1.3-μm-thick SiO_2 layer as hard mask. The etching is performed in a Sentech SI-500 ICP system, at a chuck temperature of 150 °C. We have used a highly anisotropic etching process based on HBr and O_2 (ratio 20:3, at a pressure of 2.5 mTorr), with a coil power of 1000 W and a dc bias of 400 V. These etching conditions yield an etch rate of 1.5 μm/min. The whole sample was then passivated with a 500-nm-thick SiO_2 layer, which was etched on the top of the laser ridges to allow electrical contacts and also shaped into diffraction gratings at the proper positions on the sample. A Ti/Au metallization (5/200-nm-thick) was then evaporated to provide both the electrical contacts on the top of the laser ridges and the SPP-carrying layer. The diffraction gratings, which are etched into the SiO_2 layer, are second-order gratings (lattice spacing $= \lambda_{spp}$) and consist of seven periods. After polishing and deposition of the back-contact, the samples were cleaved and In-soldered onto copper blocks for electro-optical characterizations.

Figure 2(a) shows the applied bias and the optical power (collected from a cleaved facet) as a function of the injected current for a 1.3-mm-long laser ridge at room temperature. The corresponding laser spectrum is shown in Fig. 2(b). The laser threshold current density is $J_{th} \approx 3.5\ kA/cm^2$. This value is almost twice as high as for a laser with two cleaved facets and of the same length (data not shown). The threshold increase is possibly due to the reduced reflectivity of the nonperfectly vertical dry-etched laser facets.

We have used a microbolometer mid-IR camera with a home-built imaging system based on antireflection-coated

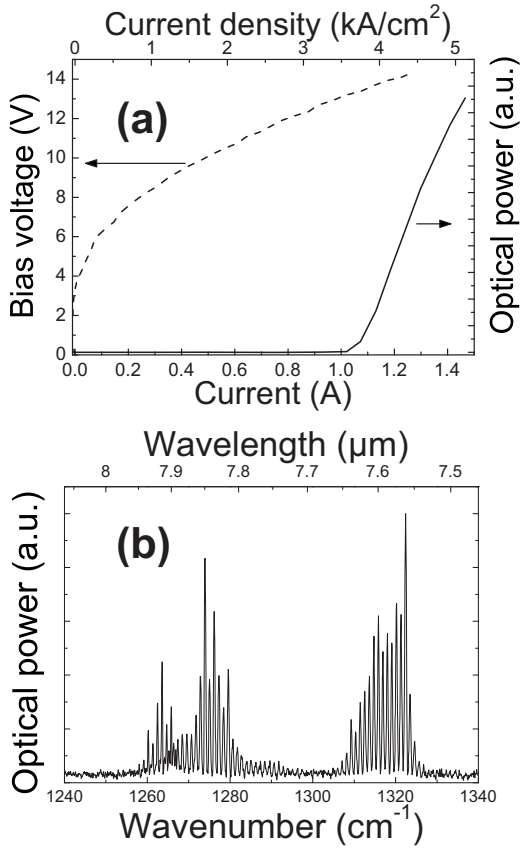

FIG. 2. (a) Current-voltage and light-current characteristics at 300 K for a typical device. The laser ridge dimensions are 1300 $\mu m \times 22\ \mu m$. (b) Emission spectrum of the same device, acquired at 300 K just above the laser threshold. These measurements are performed under pulsed current injection (50 ns duration and 84 kHz repetition rate).

germanium lenses to detect and visualize the photons originating from the scattering of SPPs off the metal gratings. Figures 3(a) and 3(b) show images of two different devices with and without metallic SPP waveguide at the laser edge, respectively. The second one (panel b) is the reference de-

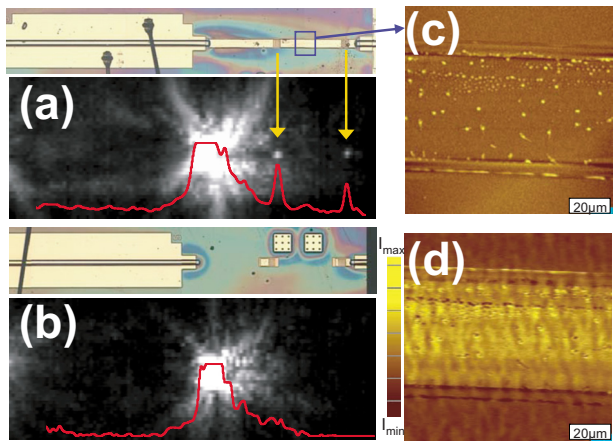

FIG. 3. (Color online) Microbolometer IR camera images (in grayscale) of two devices in operation, (a) one with and (b) one without a SPP gold-strip waveguide at the laser facet. The corresponding optical image is shown above each IR image. The devices include two diffraction gratings located at 500 and 1000 μm from the laser facet. The lines show the intensity profile along the metal strip for the device with SPP waveguide and in the corresponding area for the device without. Panels (c) and (d) show the topography (AFM signal) and the near-field intensity (i) (a-NSOM signal) corresponding to the blue square zone ($100\ \mu m \times 100\ \mu m$) in panel (a).

vice. Two metal gratings were positioned at 500 and 1000 μm from the output facet of the laser, respectively. The camera snapshot in Fig. 3(a) shows an intense central spot which corresponds to light scattered at the laser facet. The two smaller spots on the right, highlighted by the yellow arrows, correspond to light originating from SPPs that are scattered off the metal gratings. The solid line in Fig. 3(a) is a one-dimensional section of the infrared image (The gray scale of the pixels along the metal strip is represented). The clear absence of light diffraction at the grating locations in the *reference* device [Fig. 3(b)] proves that in Fig. 3(a), the electromagnetic energy is transferred to the localized probes via the metal waveguide. Note that, as shown in the diagram in Fig. 1(a), the diffraction gratings are *fully* metalized, sides and bottom included, and the metal thickness is several times larger than the gold skin depth which is $\approx$10 nm at $\lambda = 7.5$ μm wavelength. This guarantees that the photons originating from the diffraction grating cannot originate from unwanted leakage of stray-modes guided, for instance, in the substrate. Furthermore, the lack of signal originating from the region in between the two gratings [Fig. 3(a)] demonstrates the nonradiating character of the waves that mediate the energy transfer, typical of SPPs.

A quantitative experimental estimate of the SPP attenuation coefficient can be obtained from the camera image in Fig. 3(a) and it yields $\alpha_{SPP} \approx 5.5$ cm^{-1}. This value is roughly one order of magnitude higher than what is expected from a theoretical estimate of the SPP decay length at $\lambda_0 = 7.5$ μm on a plain gold surface, which gives $\approx$2.6 cm.[6] The discrepancy is possibly due to the (unwanted) presence of micron-sized and submicron-sized metallic droplets on the surface of the plasmonic waveguide [Fig. 3(c)], which act as scattering centers and increase the SPP propagation losses, and to the scattering losses induced by the diffraction gratings. The value of $\approx$5.5 cm^{-1} represents therefore an upper limit for the SPP attenuation coefficient.

We have also directly detected the EM field intensity at the device surface using a custom-built, apertureless near-field scanning optical microscope[14] (a-NSOM) able to operate in the mid-IR range of the EM spectrum.[15,16] Figures 3(c) and 3(d) show the atomic force microscopy (AFM) topography of a portion of the metal waveguide [corresponding to the square zone in Fig. 3(a)], and the intensity of the electromagnetic near-field when the device is in operation, respectively. A surface wave is clearly measured on the surface of the metal strip, while no signal is detected in the region where the metallization is absent. The near-field signal stems from the presence of a SPP wave which is launched by the laser device into the passive waveguide and propagates along it. The *direct* observation of a SPP wave on the metallic surface complements and further corroborates the detection obtained with far-field techniques.

In conclusion, we have demonstrated a compact mid-IR, SPP coupling system based on an integrated, end-coupled quantum cascade laser. Infrared imaging and near-field measurements unambiguously prove the generation of SPPs propagating along a metal-air interface. This device is particularly valuable in the mid-IR range of the EM spectrum, where it could constitute an important building-block for semiconductor-based breadboards which would allow easy testing of plasmonic concepts at very long wavelengths.

We thank G. Tessier (ESPCI), R. Braive (LPN), and D. Chouteau (LPN) for technical help. The device fabrication has been performed in part at the CTU-IEF-Minerve which was partially funded by the "Conseil Général de l'Essonne." This work was conducted as part of a EURYI scheme award. See www.esf.org/euryi. This work was also supported by the French National Research Agency (Grant Nos. ANR-09-NANO-020 "Gospel" and ANR-07-NANO-039 "NanoFTIR") and the C'Nano Ile de France (PSTS).

[1] M. I. Stockman, Phys. Rev. Lett. **93**, 137404 (2004).
[2] D. O'Connor, M. McCurry, B. Lafferty, and A. V. Zayats, Appl. Phys. Lett. **95**, 171112 (2009).
[3] S. I. Bozhevolnyi, V. S. Volkov, E. Devaux, J. Y. Laluet, and T. W. Ebbesen, Nature (London) **440**, 508 (2006).
[4] J. B. Pendry, L. Martín-Moreno, and F. J. Garcia-Vidal, Science **305**, 847 (2004).
[5] S. A. Maier, S. R. Andrews, L. Martín-Moreno, and F. García-Vidal, Phys. Rev. Lett. **97**, 176805 (2006).
[6] S. A. Maier, *Plasmonics: Fundamentals and Applications* (Springer, New York, 2007).
[7] A. Babuty, A. Bousseksou, J.-P. Tetienne, I. Doyen, C. Sirtori, G. Beaudoin, I. Sagnes, Y. De Wilde, and R. Colombelli, Phys. Rev. Lett. **104**, 226806 (2010).
[8] C. S. Kim, I. Vurgaftman, R. A. Flynn, M. Kim, J. R. Lindle, W. W. Bewley, K. Bussmann, J. R. Meyer, and J. P. Long, Opt. Express **18**, 10609 (2010).
[9] C. Pang, F. Gesuele, A. Bruyant, S. Blaize, G. Lérondel, and P. Royer, Opt. Express **17**, 6939 (2009).
[10] The commercial software COMSOL MULTIPHYSICS was employed for the numerical simulation.
[11] A. Michon, R. Hostein, G. Patriarche, N. Gogneau, G. Beaudoin, A. Beveratos, I. Robert-Philip, S. Laurent, S. Sauvage, P. Boucaud, and I. Sagnes, J. Appl. Phys. **104**, 043504 (2008).
[12] M. Bahriz, V. Moreau, J. Palomo, R. Colombelli, D. A. Austin, J. W. Cockburn, L. R. Wilson, A. B. Krysa, and J. S. Roberts, Appl. Phys. Lett. **88**, 181103 (2006).
[13] A. Dousse, J. Suffczynski, R. Braive, A. Miard, A. Lemaitre, I. Sagnes, L. Lanco, J. Bloch, P. Voisin, and P. Senellart, Appl. Phys. Lett. **94**, 121102 (2009).
[14] Y. De Wilde, F. Formanek, R. Carminati, B. Gralak, P.-A. Lemoine, K. Joulain, J.-P. Mulet, Y. Chen, and J.-J. Greffet, Nature (London) **444**, 740 (2006).
[15] P.-A. Lemoine, V. Moreau, M. Bahriz, Y. De Wilde, R. Colombelli, L. R. Wilson, and A. B. Krysa, Mater. Sci. Eng., B **149**, 270 (2008).
[16] V. Moreau, P. A. Lemoine, M. Bahriz, Y. De Wilde, R. Colombelli, L. Wilson, and A. Krysa, Appl. Phys. Lett. **90**, 201114 (2007).